nature photonics

LETTERS

PUBLISHED ONLINE: 24 NOVEMBER 2013 | DOI: 10.1038/NPHOTON.2013.311

Photocurrent generation in semiconducting and metallic carbon nanotubes

Maria Barkelid* and Val Zwiller

The fundamental mechanism underlying photocurrent generation in carbon nanotubes[1–3] has long been an open question. In photocurrent generation, the temperature of the photoexcited charge carriers determines the transport regime by which the electrons and holes are conducted through the nanotube. Here, we identify two different photocurrent mechanisms for metallic and semiconducting carbon nanotube devices with induced p–n junctions[4–7]. Our photocurrent measurements as a function of charge carrier doping demonstrate a thermal origin[8,9] for metallic nanotubes, where photo-excited hot carriers give rise to a current. For semiconducting nanotubes we demonstrate a photovoltaic mechanism[10–12], where a built-in electric field results in electron–hole separation. Our results provide an understanding of the photoresponse in carbon nanotubes, which is not only of fundamental interest but also of importance for designing carbon-based, high-efficiency photodetectors and energy-harvesting devices.

To develop sophisticated photonic devices[13–15], the physical processes governing the electro-optical response must be understood. The process of photocurrent generation has been widely studied in both supported[4,5] and suspended[6,7] carbon nanotubes, but its origin remains controversial. Two mechanisms compete in carbon nanotubes, the photovoltaic effect[10–12], where photocurrent arises from an electric field, and the photothermal effect[8,9], where the photocurrent results from a difference in Seebeck coefficients.

Recent studies have established a fingerprint technique for distinguishing between the photothermal and photovoltaic effects in graphene[16–18]. This technique assigns a six-fold-symmetric pattern in the doping-dependent photocurrent response to the photothermoelectric effect and a two-fold symmetry to the photovoltaic effect. Here, we perform doping-dependent photocurrent measurements on individually suspended carbon nanotube devices to investigate the generation of photocurrent.

Figure 1a illustrates a nanotube suspended between two metal electrodes, where two local gates were used for remote electrostatic doping[6,19] (see Methods). Measurements were performed on three metallic and five semiconducting individual carbon nanotube p–n junctions at room temperature under vacuum.

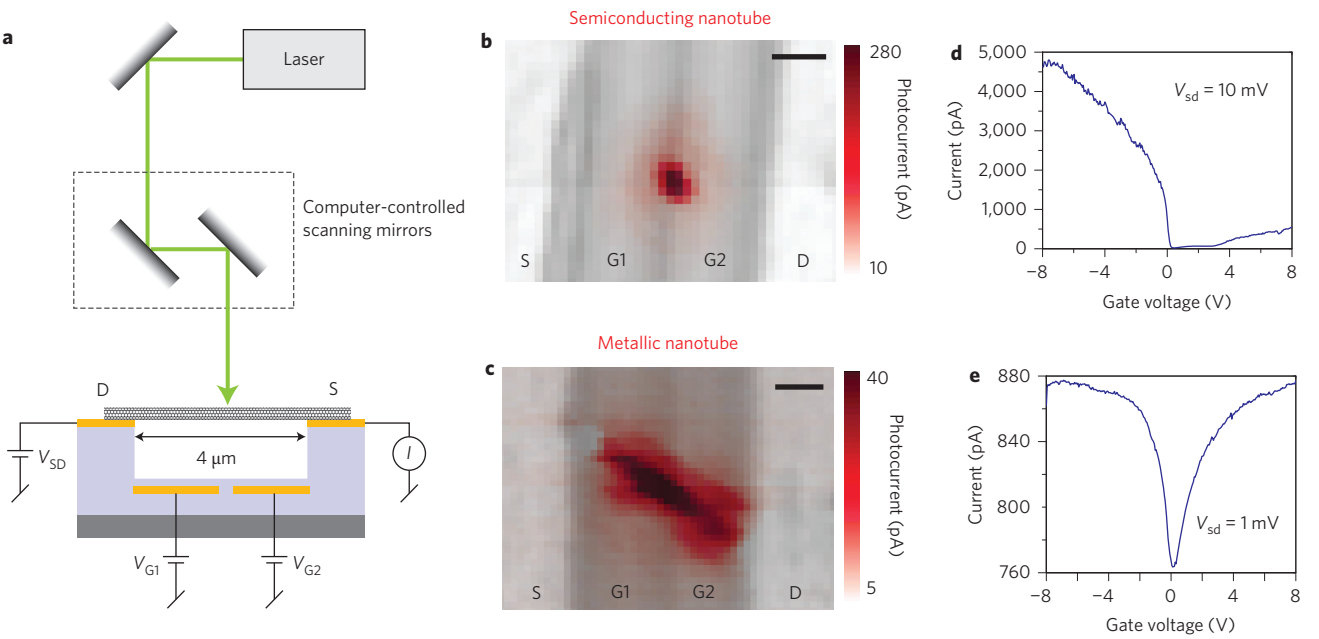

Figure 1 | SPCM and electrical characterization of semiconducting and metallic carbon nanotube devices. a, Schematic of the experimental set-up and device geometry, showing the electrical connections to the nanotube. **b**, SPCM image (at 532 nm) of the semiconducting nanotube p–n junction. The photocurrent (red) and reflection (grey) images are superimposed and show photocurrent generation from the centre of the trench. **c**, SPCM image of the metallic carbon nanotube p–n junction, showing the photoresponse from the whole body of the carbon nanotube. **d**, Electrical transfer characteristic of the semiconducting nanotube, showing a clear pinch-off of the conductance. Data were recorded with 10 mV source–drain bias. **e**, Transfer characteristic of the metallic nanotube recorded at 1 mV bias. The conductance cannot be completely quenched using gate voltage. Scale bars, 1 μm.

Kavli Institute of Nanoscience, Delft University of Technology, Lorentzweg 1, 2628 CJ Delft, The Netherlands. *e-mail: k.m.barkelid@tudelft.nl

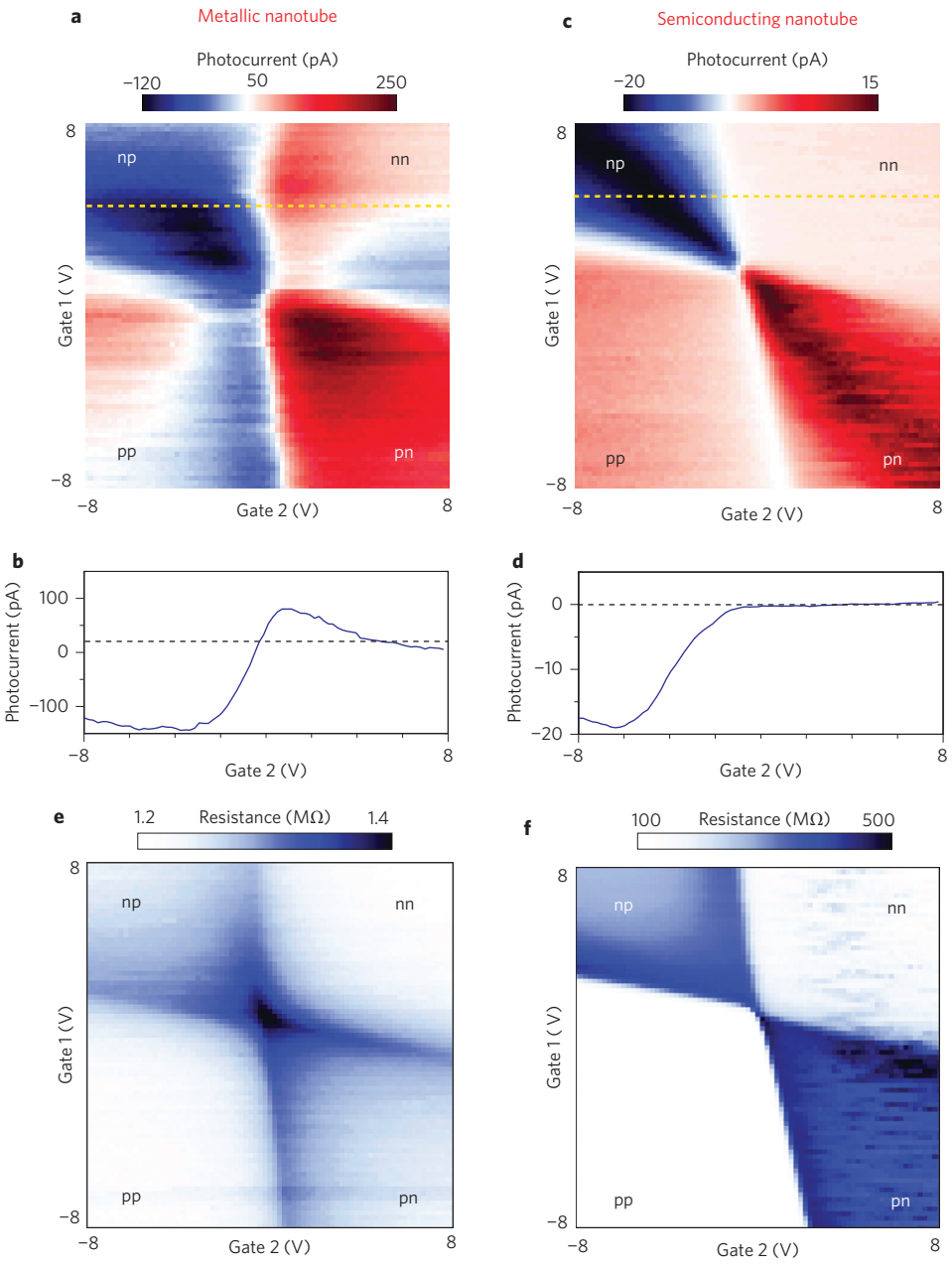

Figure 2 | Gate-dependent conductivity. a, Photocurrent map of a metallic nanotube, displaying a six-fold pattern characteristic of the photothermal effect. **b**, Line profile of the photocurrent along the yellow line in **a**, showing the multiple sign changes of the photocurrent as a function of gate voltage. **c**, Photocurrent map of a semiconducting nanotube, displaying a two-fold pattern characteristic of the photovoltaic effect. **d**, Line profile of the photocurrent along the yellow line in **c**, clearly showing a single sign change of the photocurrent as a function of gate voltage. **e**, Resistance as a function of gate voltage for the metallic nanotube. The high-resistance ridges agree with the vertical and horizontal sign changes in the photocurrent map in **a**. **f**, Resistance map for the semiconducting nanotube. The transition between high- and low-conductance regions corresponds to the transitions in the photocurrent map in **c**.

Scanning photocurrent microscopy (SPCM)[4,10,11] images of semiconducting and metallic nanotube p–n junctions (gate voltage, ± 8 V), with zero source–drain bias, were obtained with a 532 nm (1.45 kW cm^{-2}) laser. The photocurrent and reflection images were superimposed, generating Fig. 1b and c. The semiconducting nanotube in Fig. 1b shows photocurrent generated at the p–n junction formed between the two gates. The photocurrent from the metallic nanotube p–n junction in Fig. 1c has a much broader distribution, possibly a result of inefficient coupling to phonons[20], resulting in a thermal gradient extending along the nanotube due to the long electron cooling length[21].

The transfer characteristics of the two nanotubes are shown in Fig. 1d,e. With a bias of 10 mV across the semiconducting nanotube, both gate voltages were swept from negative to positive values. The electron conductance is 10 times lower than the hole conductance due to a poor n-type contact. In the metallic nanotube, with a bias of 1 mV, the conductance could be modulated by the gate voltage, but could not be quenched.

After spatial imaging, the laser was targeted at the p–n junction and the photoresponse was recorded as a function of gate voltage ($\lambda = 532$ nm, $P = 1.45$ (2.9) kW cm^{-2} for the semiconducting (metallic) nanotube). The metallic nanotube in Fig. 2a shows a clear six-fold pattern, characteristic of the photothermal effect. As predicted and demonstrated for graphene[16,17], this characteristic pattern arises from the dependence of the photocurrent on the Seebeck coefficient S. In agreement with ref. 16, due to the close

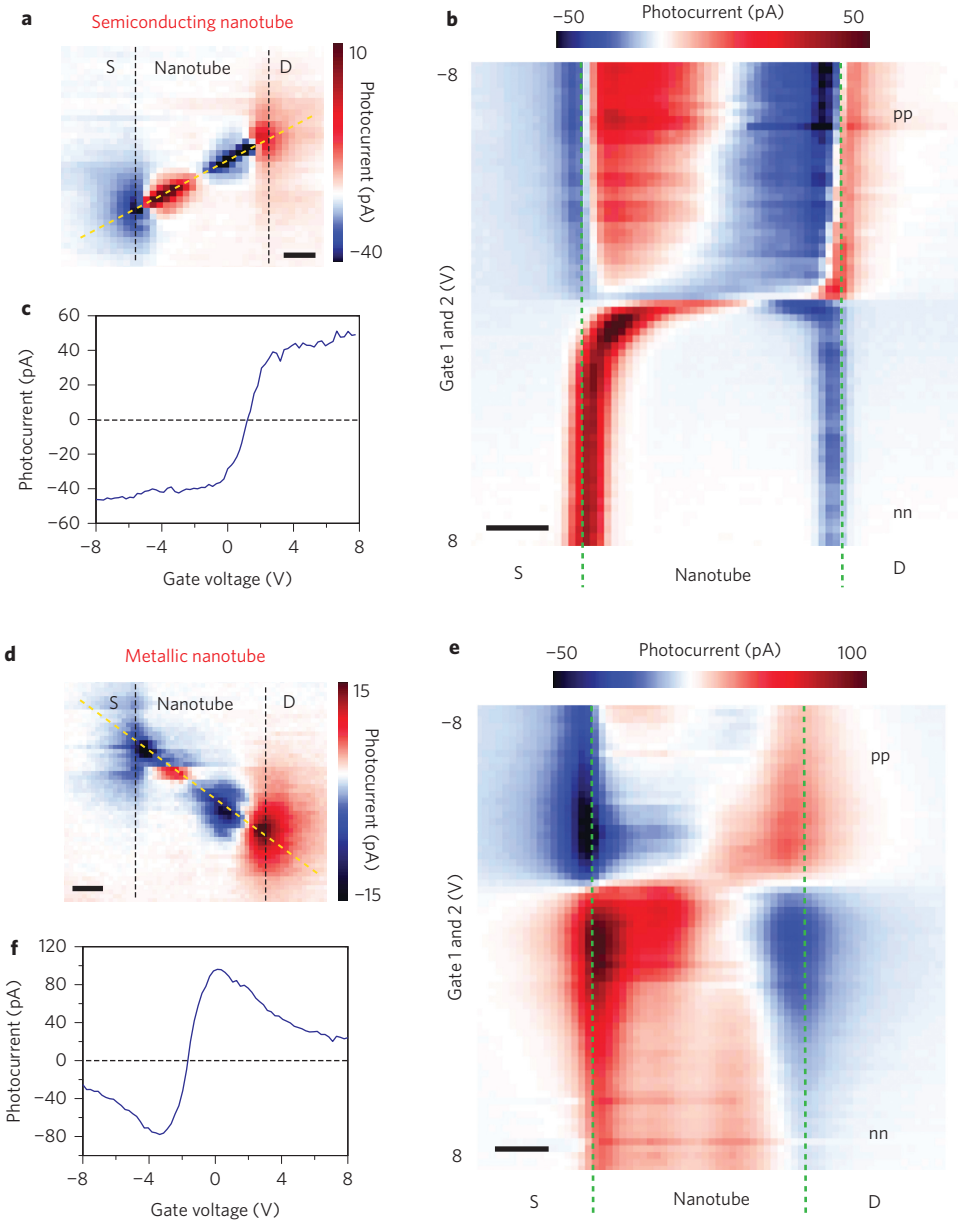

Figure 3 | Photocurrent response for homogeneous doping. a, SPCM image of the semiconducting nanotube with homogeneous p-doping. **b**, The laser is scanned along the nanotube axis (yellow line in **a**) while changing the doping from p-type to n-type. The photocurrent response shifts towards the centre of the nanotube for low doping levels. **c**, Line profile along the left green line in **b**. The photocurrent increases with gate voltage, resulting from the sign change of the electric field at the Schottky barrier. **d**, SPCM image of the metallic nanotube with p-doping. **e**, The laser is scanned along the yellow line in **d**, while tuning the gate voltage. The photocurrent from the nanotube–electrode interface shows no spatial shift with gate voltage. **f**, Line profile along the left green line in **e**. The photocurrent shows a non-monotonic trend originating from the Seebeck effect. Measurements were performed at 532 nm. All scale bars, 1 μm.

dependence on chemical potential the Seebeck coefficient has a non-monotonic dependence on gate voltage[16,22]. This results in several polarity reversals of ($S_{region2} - S_{region1}$). The photothermal current in the metallic nanotube arises from this difference in Seebeck coefficient in the two regions of the nanotube and hence displays multiple sign changes, giving rise to the six distinct regions in Fig. 2a. A line profile is presented in Fig. 2b, which demonstrates the multiple sign changes in the photocurrent. The thermally excited hot carriers decay through carrier multiplication into several low-energy electrons, leading to a local hot carrier distribution[23,24].

A photocurrent map was also recorded for the semiconducting nanotube (Fig. 2c), which displays a characteristic two-fold pattern indicative of the photovoltaic effect, where the direction of the photocurrent is parallel to the built-in electric field at the junction. An intense photocurrent signal is generated for p–n and n–p doping due to the presence of the electric field dissociating the excitons. For a homogeneously p-doped or n-doped nanotube the photocurrent is negligible, as the electric field is not sufficient to separate the exciton into free charge carriers. In the photovoltaic effect, when tuning the gate voltage, and thereby the charge carrier concentration, the sign of the electric field at the junction changes. For increasing gate voltage, the electric field only changes sign once, resulting in a single polarity change of the photocurrent. Figure 2d presents a line profile of the photocurrent as a function of gate voltage. The sign changes in the photocurrent map in

Fig. 2c do not occur exactly at zero gate voltage, as a result of the two trench gates not coupling equally to the nanotube or the semiconducting nanotube being slightly p-doped.

Our key observation from Fig. 2 is the existence of two distinctly different patterns in the photocurrent response in semiconducting and metallic nanotubes. This shows that the dominant mechanism for the generation of photocurrent differs in the two nanotubes. External factors could potentially suppress the contribution from one or both mechanisms[25,26]. Accordingly, we defined a set of experimental conditions that justify a comparison between the metallic and semiconducting nanotubes (see Methods). All nanotubes were measured under identical conditions.

We compared the conductivity in the nanotubes with and without illumination. The resistance measurements in Fig. 2e,f, were obtained from current measurements with a bias of 1 mV and 10 mV, respectively. The resistance map of the metallic nanotube shows two highly resistive ridges. This dip in conductivity, similar to that in Fig. 1e, causes a change in the Seebeck coefficient. The photocurrent in Fig. 2a arising from the difference in the Seebeck coefficient displays a polarity change for the same gate voltages. One additional polarity change is seen along the diagonal in the photocurrent map, which does not have a counterpart in the resistance map. As the doping level is homogeneous, the Seebeck coefficient is uniform along the nanotube and cannot provide a directionality for the thermally excited carriers, and hence makes no net contribution to the photocurrent.

For a homogeneously doped semiconducting nanotube, high conductivity is observed (Fig. 2f), but the photocurrent (Fig. 2c) is negligible. This is a result of the absence of a local electric field. For p–n and n–p doping the device exhibits a large resistance as well as a large photocurrent response due to the presence of an electric field at the junction.

To support the existence of different photocurrent generation mechanisms, the photocurrent response along the nanotube axis was investigated as a function of doping. The device was tuned from homogeneous p-type to n-type while scanning the laser along the nanotube axis. The laser path is indicated in Fig. 3a for p-type doping of the semiconducting nanotube. Figure 3b shows the photocurrent shifting towards the centre of the nanotube with decreasing doping[11]. This arises from a shift in the maximum electric field at the Schottky barriers towards the centre of the nanotube, resulting from the extension of the depletion region with decreasing doping concentration[27]. A line profile of the photocurrent taken along the left green line in Fig. 3b is presented in Fig. 3c, and shows a continuous increase in photocurrent with increasing gate voltage. This is an effect of the electric field at the Schottky barrier changing sign.

The metallic nanotube (shown with p-type doping in Fig. 3d) has a much less pronounced shift in the photocurrent response, as can clearly be seen in Fig. 3e. The photocurrent, originating from the difference in Seebeck coefficient of the metallic nanotube and the metal electrode, is generated when the laser is positioned at the nanotube–electrode interface. We tuned the Seebeck coefficient of our metallic nanotube with the gate voltage, causing the photocurrent to change sign. Figure 3f presents a line profile (along the left green line in Fig. 3e), and shows a non-monotonic dependence on gate voltage, characteristic of the Seebeck effect. The photocurrent responses from the nanotube–electrode interfaces show behaviour comparable to that of the photocurrent from the p–n junctions, consistent with our observations of the photothermal and photovoltaic effects dominating in metallic and semiconducting nanotubes, respectively.

We next studied the photocurrent profile as a function of position along the nanotube axis. The photocurrent from the semiconducting nanotube p–n junction is shown in Fig. 4 (blue). The electric field at the junction was probed by the incident laser with a Gaussian profile, which determines the profile of the photocurrent. The data were fitted to a Gaussian, and divided by a factor of four for clarity. The tails come from the laser spot not being perfectly diffraction-limited. The photocurrent from the metallic nanotube p–n junction is shown in red in Fig. 4. The photocurrent follows a triangular profile, centred at the p–n junction and extending ~2 μm on each side. The broad triangular shape indicates that the photogenerated carriers are hot and follow a thermal distribution through the nanotube. At the electrode–nanotube interface the photocurrent changes sign, possibly a result of band bending at the contacts or a difference in the Seebeck coefficient between the electrode and the nanotube (see Supplementary Section 3). This difference in photocurrent features confirms that the photocurrent in semiconducting nanotubes results from an electric field and in metallic nanotubes is a thermal effect.

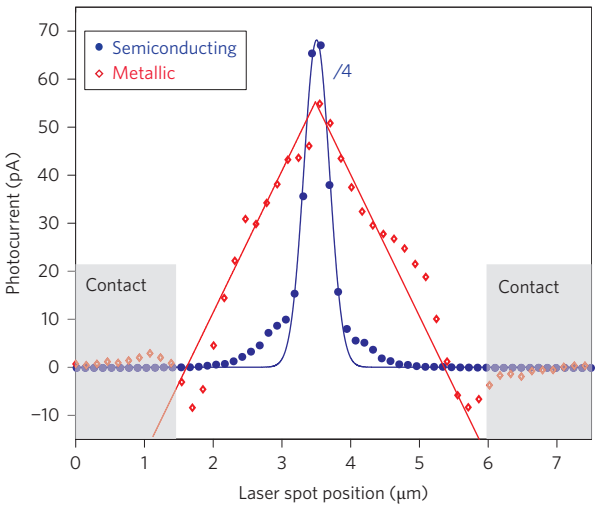

Figure 4 | Spatial photocurrent response. Photocurrent as a function of laser spot position for the semiconducting and metallic carbon nanotube p–n junctions (blue and red, respectively). The photocurrent from the semiconducting nanotube has been fitted with a Gaussian profile, originating from the laser spot profile, which is probed by the electric field at the junction. The photocurrent response from the metallic nanotube follows a triangular profile, indicating that the charge carriers stay hot until they reach the contacts, in agreement with the photothermal effect. Measurements were recorded with a 532 nm laser.

In summary, we have presented clear evidence that different photocurrent generation mechanisms dominate the photocurrent response in metallic and semiconducting nanotubes. Metallic nanotubes exhibit a dominating photothermal effect, whereas the photovoltaic effect dominates the photocurrent response in semiconducting nanotubes. A detailed understanding of the physical processes that govern photocurrent generation in carbon nanotubes is the first important step towards optimizing the design of optoelectronic devices for photodetection and energy harvesting[28,29]. This will enable highly efficient optical components based on carbon nanotubes to be engineered.

Methods

Fabrication. The device geometry was designed to individually suspend the carbon nanotubes across a trench with metal gates at the bottom of the trench. Beginning with a piece of silicon wafer covered with 285 nm thermal SiO_2, two trench gates were patterned using electron-beam lithography followed by evaporation of 5 nm tungsten and 25 nm platinum. The gates were 2 μm wide and separated by 250 nm. Next, 1 μm of SiO_2 was deposited using PECVD and the trench was created by etching away the oxide above the gate region, creating an 800-nm-deep and 4-μm-wide trench. The source and drain electrodes were defined on both sides of the trench using electron-beam lithography and metal evaporation (5 nm tungsten and 25 nm platinum). Finally, the FeMo catalyst area was patterned with electron-beam lithography on top of the metal contact, and the catalyst solution was

drop-coated onto the sample, followed by lift-off. The carbon nanotubes were grown[30] across the trench, using CH_4 and H_2 in a CVD oven at 900 °C.

Measurement set-up. The suspended carbon nanotube devices were placed in a cryostat under vacuum. Characterization was carried out by scanning the laser beam across a defined area of the sample by means of two computer-controlled scanning galvo-mirrors. The laser was focused onto the sample with an objective with a numerical aperture of 0.8. SPCM was performed and the reflected light from the sample structure was collected by a silicon photodiode. The measurements were performed at room temperature with a 532 nm continuous-wave laser.

Experimental conditions. In this study we chose a set of experimental conditions so as to make a fair comparison between semiconducting and metallic carbon nanotubes. The nanotubes were suspended to avoid heatsinking from the substrate, which suppresses the photothermal effect. The platinum contact metal was identical for all devices. To minimize the influence from defects, the nanotubes were grown in the final fabrication step and were not subjected to any post-growth fabrication. This resulted in negligible defects being present. The nanotubes were excited off-resonance. This enabled more comparable measurement conditions, as the resonances in the metallic nanotubes could not be probed. All measurements were performed at room temperature.

Received 26 April 2013; accepted 16 October 2013; published online 24 November 2013

References

1. Biercuk, M. J., Ilani, S., Marcus, C. M. & McEuen, P. L. Electrical transport in single-walled carbon nanotubes. *Top. Appl. Phys.* **111,** 455–493 (2008).
2. Dresselhaus, M. S., Dresselhaus, G., Charlier, J. C. & Hernandez, E. Electronic, thermal and mechanical properties of carbon nanotubes. *Phil. Trans. R. Soc. Lond. A* **362,** 2065–2098 (2004).
3. Dresselhaus, M. S., Dresselhaus, G., Saito, R. & Jorio, A. Exciton photophysics of carbon nanotubes. *Annu. Rev. Phys. Chem.* **58,** 719–747 (2007).
4. Freitag, M., Martin, Y., Misewich, J. A., Martel, R. & Avouris, P. H. Photoconductivity of single carbon nanotubes. *Nano Lett.* **3,** 1067–1071 (2003).
5. Gabor, N. M., Zhong, Z., Bosnick, K., Park, J. & McEuen, P. L. Extremely efficient multiple electron–hole pair generation in carbon nanotube photodiodes. *Science* **325,** 1367–1371 (2009).
6. Lee, J. U., Gipp, P. P. & Heller, C. M. Carbon nanotube p–n junction diodes. *Appl. Phys. Lett.* **85,** 145–147 (2004).
7. Barkelid, M., Steele, G. A. & Zwiller, V. Probing optical transitions in individual carbon nanotubes using polarized photocurrent spectroscopy. *Nano Lett.* **12,** 5649–5653 (2012).
8. St-Antoine, B. C., Menard, D. & Martel, R. Position sensitive photothermoelectric effect in suspended single-walled carbon nanotube films. *Nano Lett.* **9,** 3503–3508 (2009).
9. Tsen, A. W., Donev, L. A. K., Kurt, H., Herman, L. H. & Park, J. Imaging the electrical conductance of individual carbon nanotubes with photothermal current microscopy. *Nature Nanotech.* **4,** 108–113 (2008).
10. Balasubramanian, K., Burghard, M., Kern, K., Scolari, M. & Mews, A. Photocurrent imaging of charge transport barriers in carbon nanotube devices. *Nano Lett.* **5,** 507–510 (2005).
11. Ahn, Y. H., Tsen, A. W., Kim, B., Park, Y. W. & Park, J. Photocurrent imaging of p–n junctions in ambipolar carbon nanotube transistors. *Nano Lett.* **7,** 3320–3323 (2007).
12. Balasubramanian, K., Fan, Y., Burghard, M. & Kern, K. Photoelectronic transport imaging of individual semiconducting carbon nanotubes. *Appl. Phys. Lett.* **84,** 2400 (2004).
13. Mueller, T. *et al.* Efficient narrow-band light emission from a single carbon nanotube p–n diode. *Nature Nanotech.* **5,** 27–31 (2010).
14. Barone, P. W., Baik, S., Heller, D. A. & Strano, M. S. Near-infrared optical sensors based on single-walled carbon nanotubes. *Nature Mater.* **4,** 86–92 (2005).
15. Lee, J. U. Photovoltaic effect in ideal carbon nanotube diodes. *Appl. Phys. Lett.* **87,** 073101 (2005).
16. Song, J. C. W., Rudner, M. S., Marcus, C. M. & Levitov, L. S. Hot carrier transport and photocurrent response in graphene. *Nano Lett.* **11,** 4688–4692 (2011).
17. Gabor, N. M. *et al.* Hot carrier-assisted intrinsic photoresponse in graphene. *Science* **334,** 648–652 (2011).
18. Sun, D. *et al.* Ultrafast hot-carrier-dominated photocurrent in graphene. *Nature Nanotech.* **7,** 114–118 (2012).
19. Buchs, G., Barkelid, M., Bagiante, S., Steele, G. A. & Zwiller, V. Imaging the formation of a p–n junction in a suspended carbon nanotube with scanning photocurrent microscopy. *J. Appl. Phys.* **110,** 074308 (2011).
20. Pop, E. *et al.* Negative differential conductance and hot phonons in suspended nanotube molecular wires. *Phys. Rev. Lett.* **95,** 155505 (2005).
21. Strait, J. H. *et al.* Very slow cooling dynamics of photoexcited carriers in graphene observed by optical-pump terahertz-probe spectroscopy. *Nano Lett.* **11,** 4902–4906 (2011).
22. Small, J. P., Perez, K. M. & Kim, P. Modulation of thermoelectric power of individual carbon nanotubes. *Phys. Rev. Lett.* **91,** 256801 (2003).
23. Perebeinos, V. & Avouris, P. Impact excitation by hot carriers in carbon nanotubes. *Phys. Rev. B* **74,** 121410 (2006).
24. Tielrooj, K. J. *et al.* Photoexcitation cascade and multiple hot-carrier generation in graphene. *Nature Phys.* **9,** 248–252 (2013).
25. Freitag, M., Low, T., Xia, F. & Avouris, P. Photoconductivity of biased graphene. *Nature Photon.* **7,** 53–59 (2013).
26. Freitag, M., Low, T. & Avouris, P. Increased responsivity of suspended graphene photodetectors. *Nano Lett.* **13,** 1644–1648 (2013).
27. Sze, S. M. *Semiconductor Devices Physics and Technology* 225–237 (Wiley, 2002).
28. Ross, R. T. & Nozik, A. J. Efficiency of hot-carrier solar energy converters. *J. Appl. Phys.* **53,** 3813–3818 (1982).
29. Omari, M. & Kouklin, N. A. Photothermovoltaic effect in carbon nanotubes: en route toward junctionless infrared photocells and light sensors. *Appl. Phys. Lett.* **98,** 243113 (2011).
30. Kong, J., Soh, H. T., Cassell, A. M., Quate, C. F. & Dai, H. Synthesis of individual single-walled carbon nanotubes on patterned silicon wafers. *Nature* **395,** 878–881 (1998).

Acknowledgements

This research was supported by the Dutch Foundation for Fundamental Research on Matter (FOM). The authors would like to thank M.S. Rudner for discussions.

Author contributions

M.B. fabricated the devices, performed the measurements and wrote the manuscript. V.Z. supervised the project. All authors discussed the results and commented on the manuscript.

Additional information

Supplementary information is available in the online version of the paper. Reprints and permissions information is available online at www.nature.com/reprints. Correspondence and requests for materials should be addressed to M.B.

Competing financial interests

The authors declare no competing financial interests.